Article

Ice-free period too long for Southern and Western Hudson Bay polar bear populations if global warming exceeds 1.6 to 2.6 °C

Check for updates

Julienne Stroeve [1,2,3,10] ✉, Alex Crawford [1,10], Steve Ferguson [4], Ian Stirling [5,6,11], Louise Archer[7], Geoffrey York [8], David Babb [1] & Robbie Mallett[1,9]

Hudson Bay has warmed over 1 °C in the last 30 years. Coincident with this warming, seasonal patterns have shifted, with the spring sea ice melting earlier and the fall freeze-up occurring later, leading to a month longer of ice-free conditions. This extended ice-free period presents a significant challenge for polar bears, as it restricts their hunting opportunities for seals and their ability to accumulate the necessary body weight for successful reproduction. Drawing on the latest insights from CMIP6, our updated projections of the ice-free period indicate a more spatially detailed and alarming outlook for polar bear survival. Limiting global warming to 2 °C above pre-industrial levels may prevent the ice-free period from exceeding 183 days in both western and southern Hudson Bay, providing some optimism for adult polar bear survival. However, with longer ice-free periods already substantially impacting recruitment, extirpation for polar bears in this region may already be inevitable.

Hudson Bay is a seasonally ice-covered inland marginal sea of the Arctic Ocean that is home to a large population of polar bears (*Ursus maritimus*). Every July, summer sea ice retreat drives the bears onshore. During this time, they fast while relying on fat reserves until the ice re-forms in winter, allowing them to resume hunting seals from the ice[1]. Satellite observations reveal that the climatological ice-free period (IFP) was around 128 days for Hudson Bay from 1979–2014[2]. Within this region, the shortest IFP occurs in Foxe Basin and the longest IFP of 165 days within eastern Hudson Bay[3]. In western Hudson Bay (WHB) where the town of Churchill, Manitoba, is located, and one of the largest and most extensively studied polar bear populations is found, the ice-free period can be as long as 150 days[3,4].

While bears will opportunistically feed on marine mammal carcasses along the coastline[5] or possibly catch an occasional caribou during their time

on shore[6], they are mostly fasting. For every day the bears do not eat, they lose between 1 and 2 kg[7]. Historically, bears within James Bay and Hudson Bay fasted for about 4 months, or 120 days, and maintained a healthy population[1]. However, Hudson Bay is warming rapidly[8,9] (Fig. 1a–c), and the corresponding extension of the IFP[4,9] (Fig. 1d–i) has led to declining polar bear populations, especially within WHB[10,11]. This decline, observed already in the 1990s, was primarily attributed to earlier sea ice breakup[12]. Since these studies, the rate of polar bear population decline within the region accelerated, declining by 27% between 2016 and 2021 compared to 11% between 2011 and 2016[13]. The decline is largely attributed to fewer adult females, young bears, and cubs. Overall there are about half as many polar bears as in 1987 (618 vs. 1185 bears)[13], although estimates from the 1980s used different techniques and direct comparisons should be interpreted with caution[14,15].

[1]Clayton H. Riddell Faculty of Environment, Earth, and Resources, Centre for Earth Observation Modeling (CEOS), University of Manitoba, 125 Dysart Rd, Winnipeg R3T 2N2 MB, Canada. [2]Earth Sciences, University of College London, Gower Street, London WC1E 6BT, UK. [3]Cooperative Institute for Environmental Sciences (CIRES), National Snow and Ice Data Center (NSIDC), University of Colorado, 1540 30th Street, Boulder, CO 80303, USA. [4]Arctic Aquatic Research Division, Fisheries and Oceans Canada, 501 University Crescent, Winnipeg R3T 2N6 MB, Canada. [5]Biological Sciences, University of Alberta, CW 405, Biological Sciences Bldg, Edmonton T6G 2E9 AL, Canada. [6]Wildlife Research Division, Environment and Climate Change Canada, Edmonton, Alberta, Canada. [7]Laboratory of Quantitative Global Change Ecology, Department of Biological Sciences, University of Toronto Scarborough, 1265 Military Trail, Toronto M1C 1A4 ON, Canada. [8]Research and Policy, Polar Bears International, Bozeman, MT 59772, USA. [9]Earth Observation Group, Department of Physics and Technology, UiT The Arctic University of Norway, Tromsø, Troms 9019, Norway. [10]These authors contributed equally: Julienne Stroeve, Alex Crawford. [11]Deceased: Ian Stirling. ✉e-mail: Julienne.Stroeve@umanitoba.ca
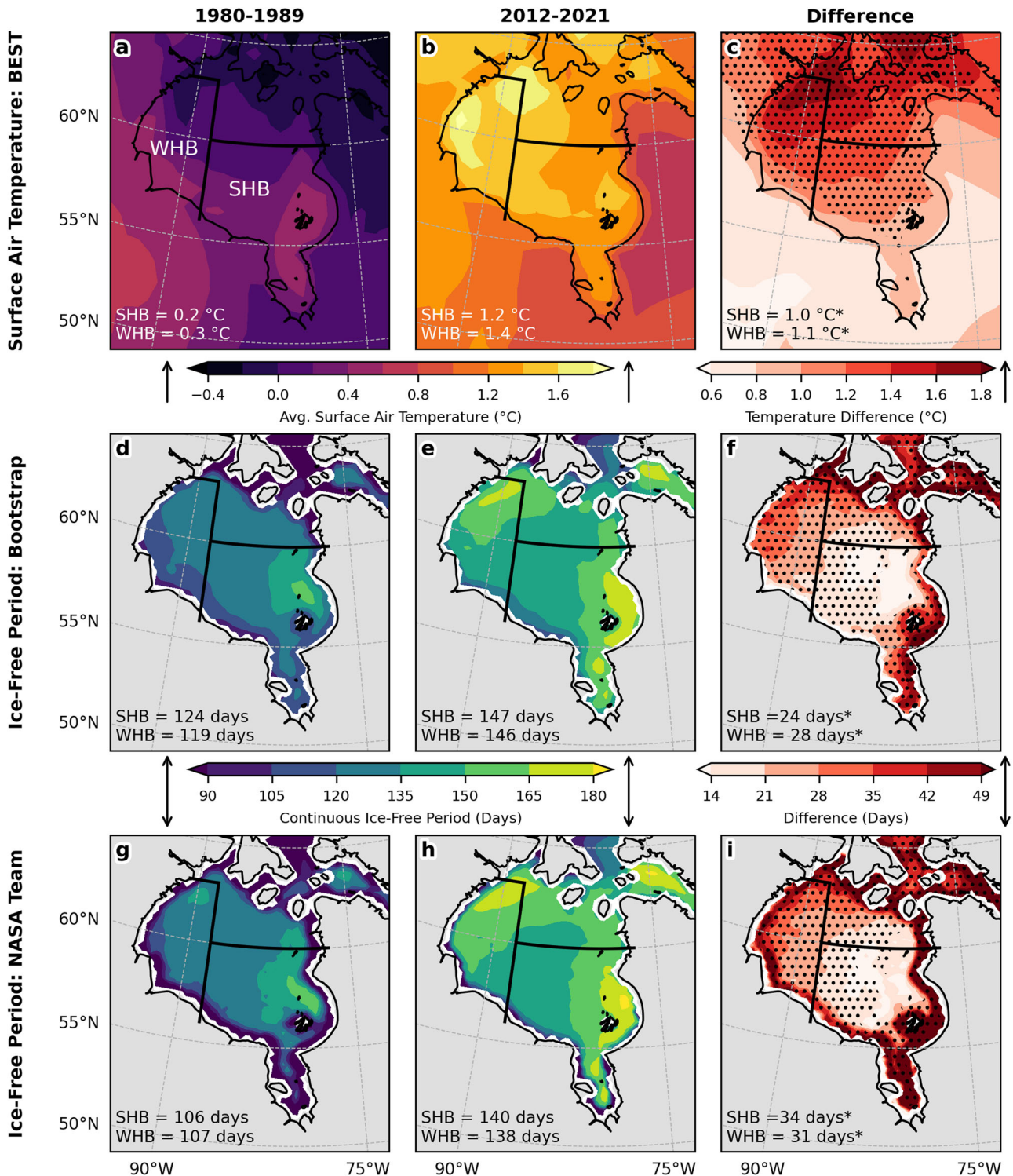
1

Fig. 1 | Change to Hudson Bay annual surface air temperature (a–c) and ice-free period (d–i) during satellite period. Temperature data is from BEST. Ice-free period is from the Bootstrap algorithm (**d–f**) and NASA Team algorithm (**g–i**), with a SIC threshold of 10%. Stippling on maps and asterisks following regional medians indicate that the differences between 1980–1989 and 2012–2021 are significant at $p < 0.05$ (two-sided) using a 2-sample Mann-Whitney test.

The most recent projections from the Intergovernmental Panel on Climate Change (IPCC) sixth assessment report[16] necessitate the re-evaluation of the future prospects of polar bears in Hudson Bay. Here we rely on model output data from version six of the Coupled Model Inter-comparison Project (CMIP6)[17] to asses future IFP changes within WHB and southern Hudson Bay (SHB) (Fig. 2g) as a function of global warming. In this study, twenty models were used for this analysis based on availability

of daily sea ice fields (see Methods in Section 5 for details). While earlier studies linked the number of days below a threshold sea ice extent with polar bear mortality[18], we redefine IFP in the models by the ice thickness. There is no scientifically documented minimum thickness of sea ice required to support an adult male polar bear. However, the choice of ice habitat by polar bears is driven more by the accessibility of ice features that enhance hunting success rather than the availability of prey[19,20]. During shoulder seasons such
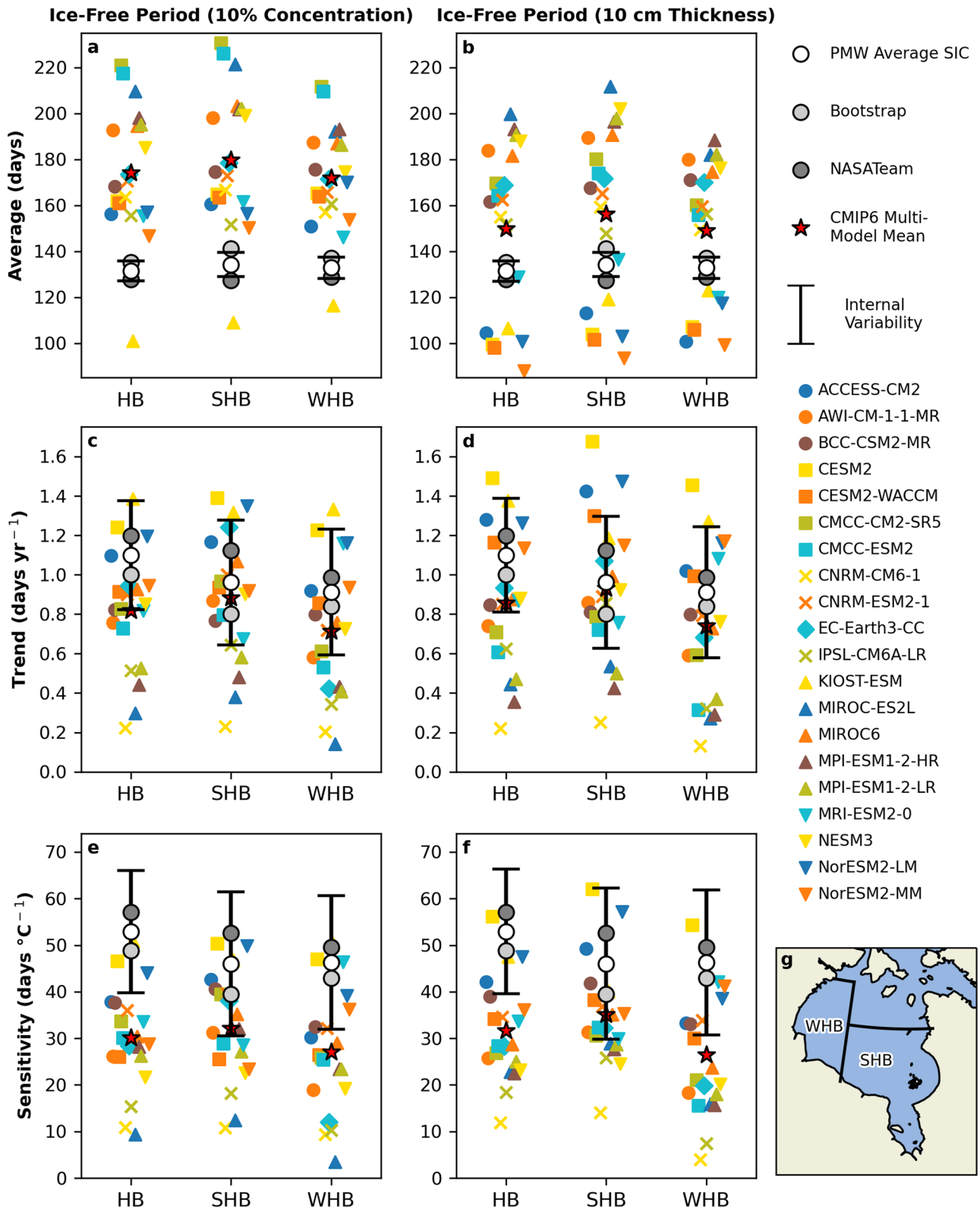
Fig. 2 | Ice-free period (IFP) derived from passive microwave (PMW) satellite SIC products and CMIP6 models. Average ice-free period (**a**, **b**), trend (**c**, **d**), and sensitivity to global annual mean surface temperature (**e**, **f**) for Hudson Bay (HB) and the western (WHB) and southern (SHB) regions (**g**). Two definitions of IFP are used for CMIP6 models: 10% SIC (left), and 10 cm sea ice thickness (right). All data are from the period 1979–2021, with the historical+SSP585 experiments used for 20 CMIP6 models. Only the first ensemble member is used for each model, and the multi-model mean is unweighted. The white dots represent the average of Bootstrap and NASA Team products. Internal variability is taken as two times the standard deviation of the 30-member ensemble from MPI-ESM1-2-LR.

Fig. 3 | Comparison of two methods for projecting ice-free period by global annual temperature anomaly. Results are shown for **a** Southern Hudson Bay and **b** Western Hudson Bay. The red line represents the weighted average of 49 CMIP6 simulations, with light red shading showing the 5–95% confidence range. The black line represents the bias-adjusted time series of 20 equally weighted model simulations (one ensemble member per model), with gray shading for the 5–95% confidence range. Darker red shading indicates that uncertainty for both methods overlaps. Gold indicates the ice-free period in the passive microwave record (PMW; 1979-2021). Vertical lines indicate the average global temperature anomaly for two historical decades.
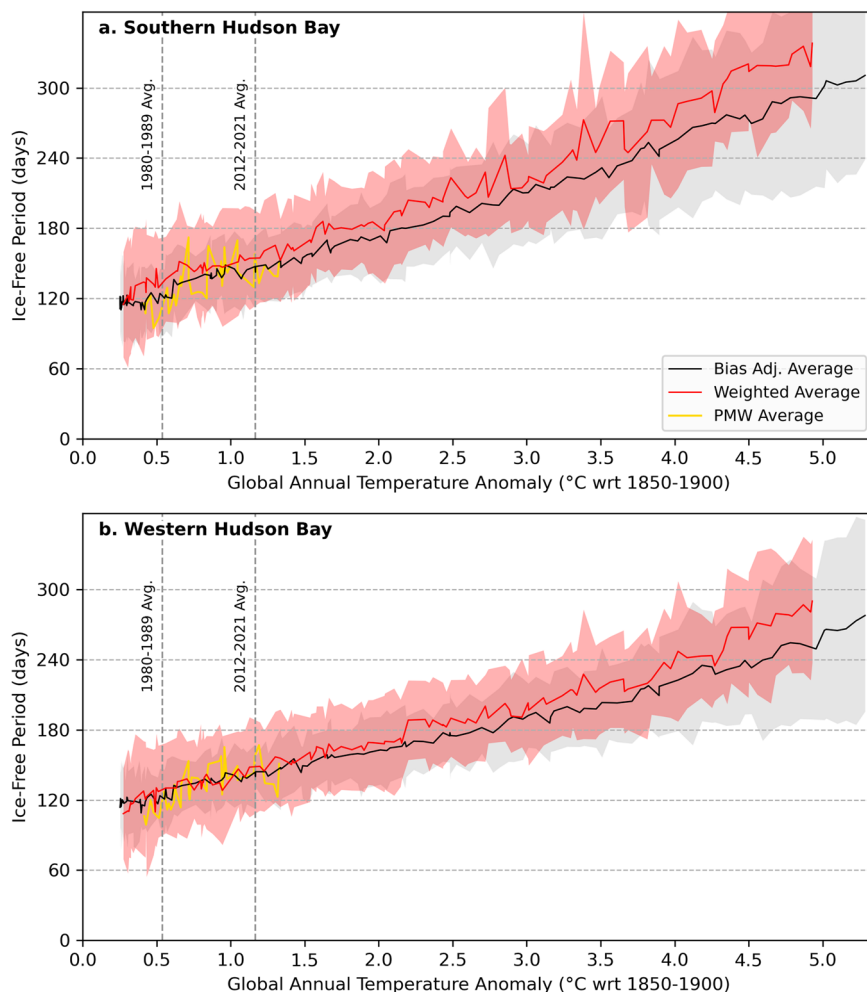
as spring break-up and autumn ice formation, polar bears exhibit a preference for new first-year ice (<30 cm thickness)[21]. Although subjective, it is reasonable to posit that a minimum thickness of at least 10 cm serves as a threshold requirement for a platform conducive to successful seal hunting[22–24]. The use of a minimum of 10 cm also aligns with the minimum thickness for the frazil ice schemes in some models (see summary of models in Table 2 of Keen et al. (2021)[25]). We believe incorporating thickness provides a more realistic representation of the environmental limits experienced by polar bears hunting seals from the ice surface[21].

The selection of a 10 cm ice thickness threshold for defining the IFP in the CMIP6 models aligns more accurately with observed IFPs obtained through satellite estimates of sea ice concentration (SIC), when combined with a 10% SIC threshold (see Methods in Section 5 for details). Using the same SIC threshold leads to a significant overestimation of the IFP (Fig. 2a), on average by 50 days. When using a 10 cm ice thickness threshold to define the IFP, the bias of the multi-model mean is reduced to about 30 days (Fig. 2b).

Models perform better at capturing the 1979-2021 trends in IFP (Fig. 2c, d). The multi-model ensemble mean trend aligns closely with the lower end of the observed internal variability for Hudson Bay overall. This implies that although a mean bias exists in the IFP duration, the models generally represent the rate of change observed over the satellite data record. However, this agreement in trends occurs because of two counteracting biases in the models. First, the sensitivity of the IFP to global annual mean temperature is considerably weaker in most of the models than in observations (Fig. 2e, f). Second, many CMIP6 models overestimate the rate of global warming in the historical period[26]. Underestimation of temperature sensitivity counteracts overestimation of warming rates, which leads to

accurate trends. A similar effect is found for simulated trends in Arctic-wide sea ice extent[27].

Future projections
To address model biases, we present two sets of projections for future IFPs. First, a delta-shift bias adjustment is applied to the first ensemble member of each of the 20 CMIP6 models based on the difference between modeled and satellite-based IFPs. These 20 simulations (Supplementary Table 1) are then averaged with equal weight. Second, we apply a weighted average of 49 simulations from the 20 models, accounting for both model performance and independence with regard to both sea ice and temperature averages and trends. More weight is given to models with shorter IFPs and stronger sensitivity of IFP to warming (see Methods in Section 5 for details). For the following results, the bias-corrected result is always listed first, and the weighted average is given in parentheses.

Future projections begin similarly at about 120 (120) days for each region (at 0.5 °C of global warming relative to 1850–1900), yet the weighted average shows a slightly faster pace of increase per degree of global warming (Fig. 3; Supplementary Table 2) Because the bias-adjustment method shifts all model results to equal the observational average, uncertainty for the ice-free period at lesser levels of global warming is lower than for the weighted average. However, the uncertainty for the two methods converges for greater levels of global warming. For example, at 4 °C, the uncertainty is 43 (44) days for WHB and 63 (61) days for SHB. Compared to WHB, SHB exhibits both higher uncertainty and a faster increase in IFP.

Projected increases in IFP occur both because of earlier sea ice retreat in spring/summer and later sea ice advance in autumn (Fig. 4). Based on the

Fig. 4 | Regional averages of seasonal sea ice retreat and advance dates, which bookend the ice-free period. Results are shown for **a** Southern Hudson Bay and **b** Western Hudson Bay. Blue represents the bias-adjusted average of 20 CMIP6 simulations (one ensemble member per model) and red represents a weighted average of 49 CMIP6 simulations. Average values are shown for global annual temperature anomalies (with respect to 1850–1900) from the SSP585 simulations. Gray circles on the left-hand side show bias-adjusted average April snow depth from the same 20 CMIP6 simulations.
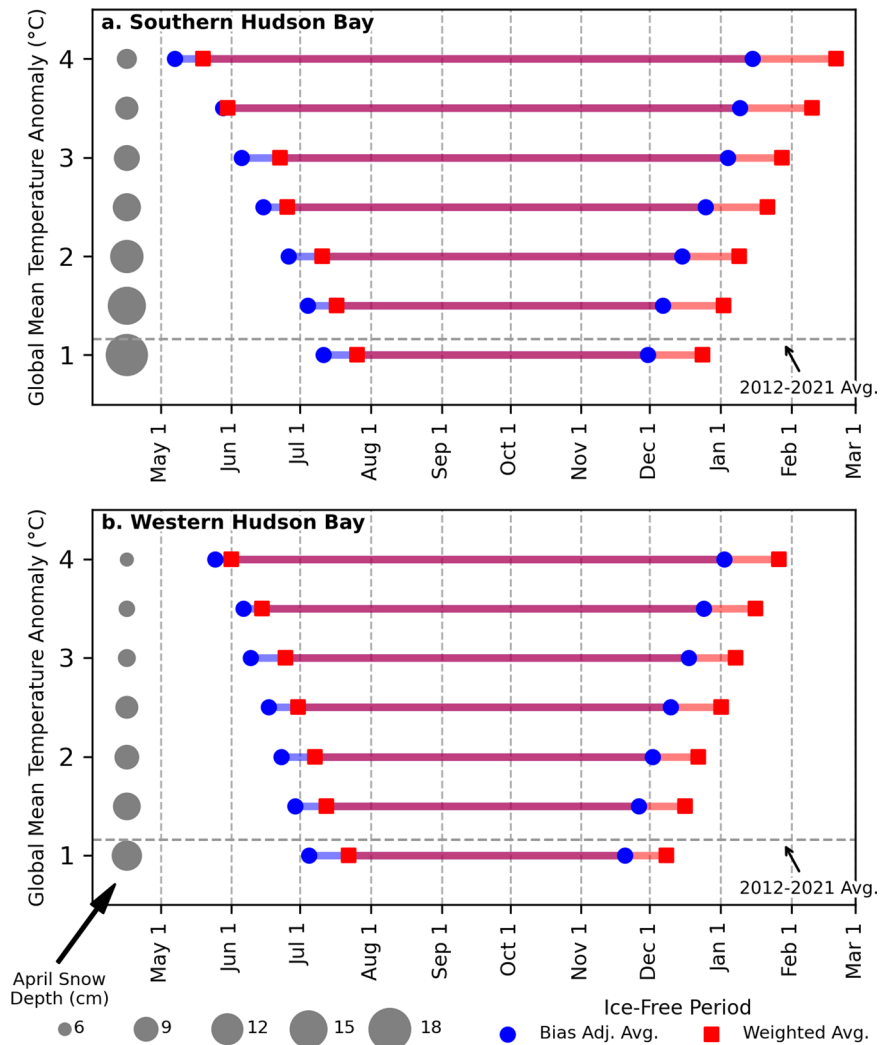
CMIP6 multi-model averages, the retreat typically occurs in mid (late) July and advance in early (late) December in SHB at 1 °C of global warming (corresponding roughly to the period 2000–2019). Both retreat and advance occur about a week or two earlier in WHB than SHB. This results in an average IFP of about 140 (150) days in SHB and about 140 (140) days in WHB; however, the weighted average shows a shift of the entire IFP by about two weeks later. At 1.5 °C of global warming the IFP increases by about two weeks in both regions: 155 (170) days in SHB and 150 (155) days in WHB, with the bias-adjusted retreat day shifting to about July 1. At 2 °C, the SHB and WHB ice-free period averages about 175 (180) and 165 (170) days, respectively. The timing of retreat is now late June (early July) in both regions, and advance occurs in mid December (early January) in SHB and early December (late December) in WHB.

Using the SSP5-8.5 scenario (the most pessimistic emission scenario resulting in additional radiative forcing of 8.5 Wm⁻² by 2100), all model simulations surpass 4 °C of global warming before the end of the century, but even in the more moderate SSP3-7.0 emissions scenario, 4 °C is still the multi-model mean[16]. Reaching 4 °C yields an average IFP around 255 (280) days per year in SHB - roughly 100 days longer than at 1.5 °C. Sea ice retreat in SHB is in early May (late May), and advance is in mid-January (mid-February). Using either method, the increase in IFP comes roughly equally from earlier retreat and later advance, but the weighted average undergoes faster change in all metrics. In WHB, 4 °C of global warming means 220 (240) ice-free days per year, which represents a more modest increase of about 70 (85) days compared to 1.5 °C. Retreat is before June (around June) and advance occurs in early January (late January).

These regional averages mask important local changes, such as the spatial gradient that develops, with the shortest ice-free periods occurring in the west and the longest ice-free periods occurring in the southeast (Fig. 5). This gradient is more pronounced with increased warming, where the difference between the east and west extends from about one month at 2 °C to two months at 4 °C. In the southeast, the average ice-free period exceeds 300 days at 4 °C.

Snow depth and seal pup survival

Hudson Bay provides a year-round home to 3 species of seals (Phocidae), which include ringed (*Pusa hispida*), harbour (*Phoca vitulina*) and bearded seals (*Erignathus barbatus*); seasonally, the harp (*Pagophilus groenlandicus*) and hooded (*Cystophora cristata*) seals occupy the northern part of Hudson Bay during the ice-free season but largely occur in open water where they are inaccessible to polar bears. Ringed seals, and to a lesser degree bearded seals are primary prey for the polar bears in WHB and SHB, while harbour seals provide a minor food source[28], as they are limited to relatively shallow coastal waters[29]. The polar bears' most abundant prey, ringed seals, have a relatively high density occupying the landfast ice that forms along the coast and the nearby offshore pack ice. In April, females dig subnivean lairs over breathing holes they have maintained through the winter beneath drifted snow over areas of rough ice or along pressure ridges[30,31]. These structures reduce the risk of predation by polar bears during this vulnerable period and protect pups from cold weather because their fur and fat layers are not yet sufficiently developed to provide adequate insulation from the cold[32].
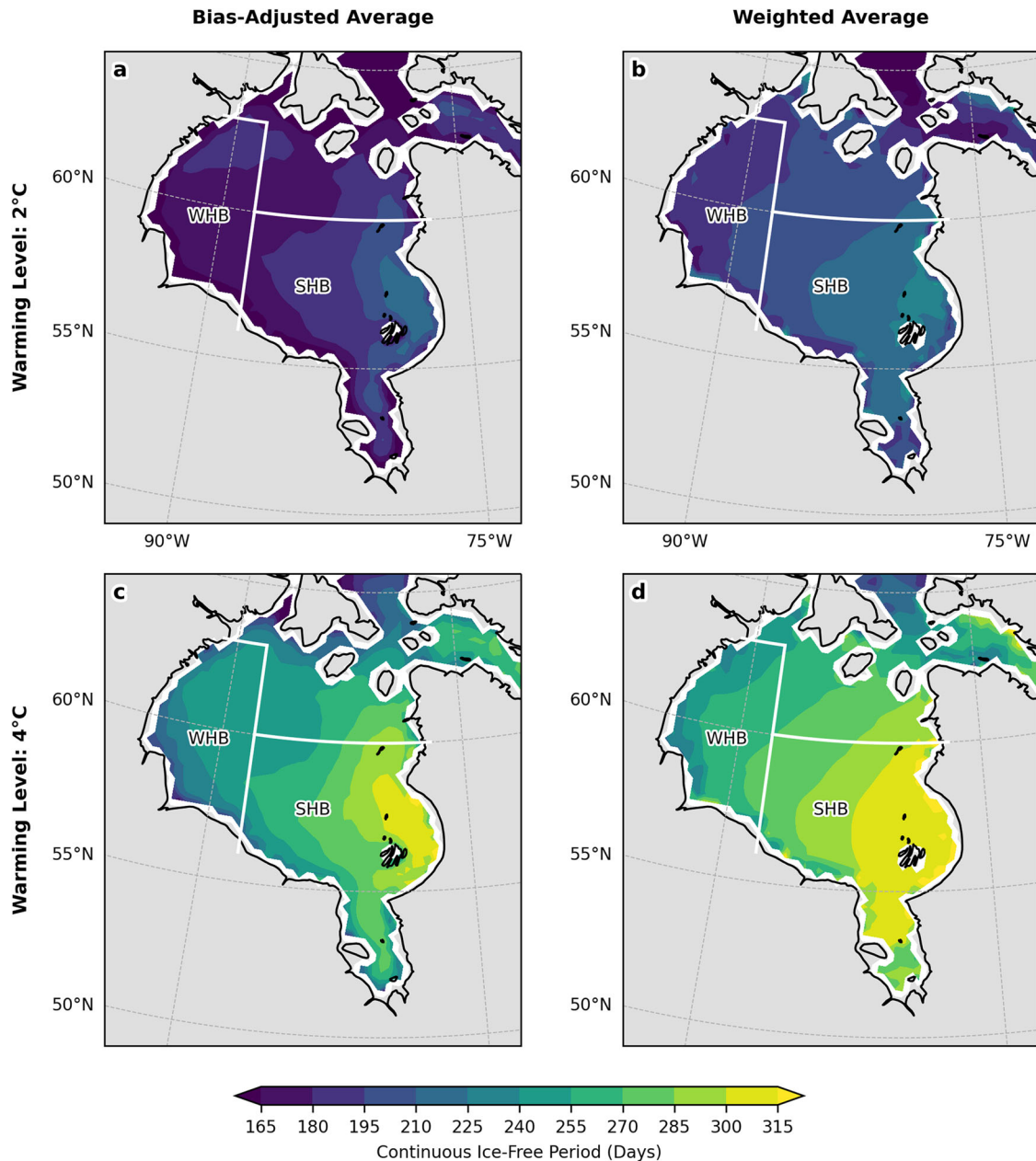
Fig. 5 | Comparison of the average ice-free period at different temperature thresholds and under different averaging schemes. a, b indicate ice-free period at 2 °C of global warming and (**c, d**) at 4 °C of global warming (with respect to 1850–1900) using the **a, c** bias-adjusted average and **b, d** weighted average of CMIP6 simulations.

Following parturition, female ringed seals nurse their pups for about 40 days, during which they are most vulnerable to polar bear predation[22].

The depth of snow on the sea ice in April when the birth lairs are dug by female ringed seals is critical to the survival of pups[33] and thus the reproductive success of the polar bears that depend on them. Under normal conditions, the average height of a birth lair is 31–32 cm[30,31] and the total depth of the snow containing the lair may be up to approximately double those values. In most areas, birth lairs are not common in areas of open relatively flat ice, though there may be breathing holes present[22,31,32].

However, when sea ice forms later, there is less time for snow to form into hard windblown drifts suitable for birth lairs in adjacent areas of rough ice or pressure ridges. While less snow cover may provide more opportunities for polar bears to access ringed seal birth lairs, it also poses a heightened risk to the pups. If the depth of snow in drifts declines, seal pups may be at increased risk of predation or freezing[32]. Snow depths below 32 cm are associated with decreased seal pup survival[34].

Unlike sea ice phenology, CMIP6 models exhibit no substantial bias in April snow depth on sea ice (Fig. 6a–c). Several models overestimate snow depth and several underestimate, but the regionally averaged multi-model mean is almost a perfect match to observations without weighting or adjustment (note how the white circle largely covers the red star). CMIP6 also correctly portrays a gradient of thicker snow cover in the southeast and thinner snow cover in the northwest, although snow depth in the central part of Hudson Bay (part of SHB) is generally too thin. This is counterbalanced by snow depth in James Bay and southeastern Hudson Bay being higher in CMIP6.

Models forecast a modest decline in snow depth for WHB (about 2 cm °C⁻¹) and a stronger decline in SHB (3 to 4 cm °C⁻¹) (Fig. 4, gray circles, Fig. 6d, e). The thickest snowpacks also shift from being on the east side of Hudson Bay to being in the center and on the west side. At 1 °C, average April snow depth is 11 cm in WHB and 17 cm in SHB. At 4 °C, average April snow depth is 7 cm in WHB and only 6 cm in SHB.
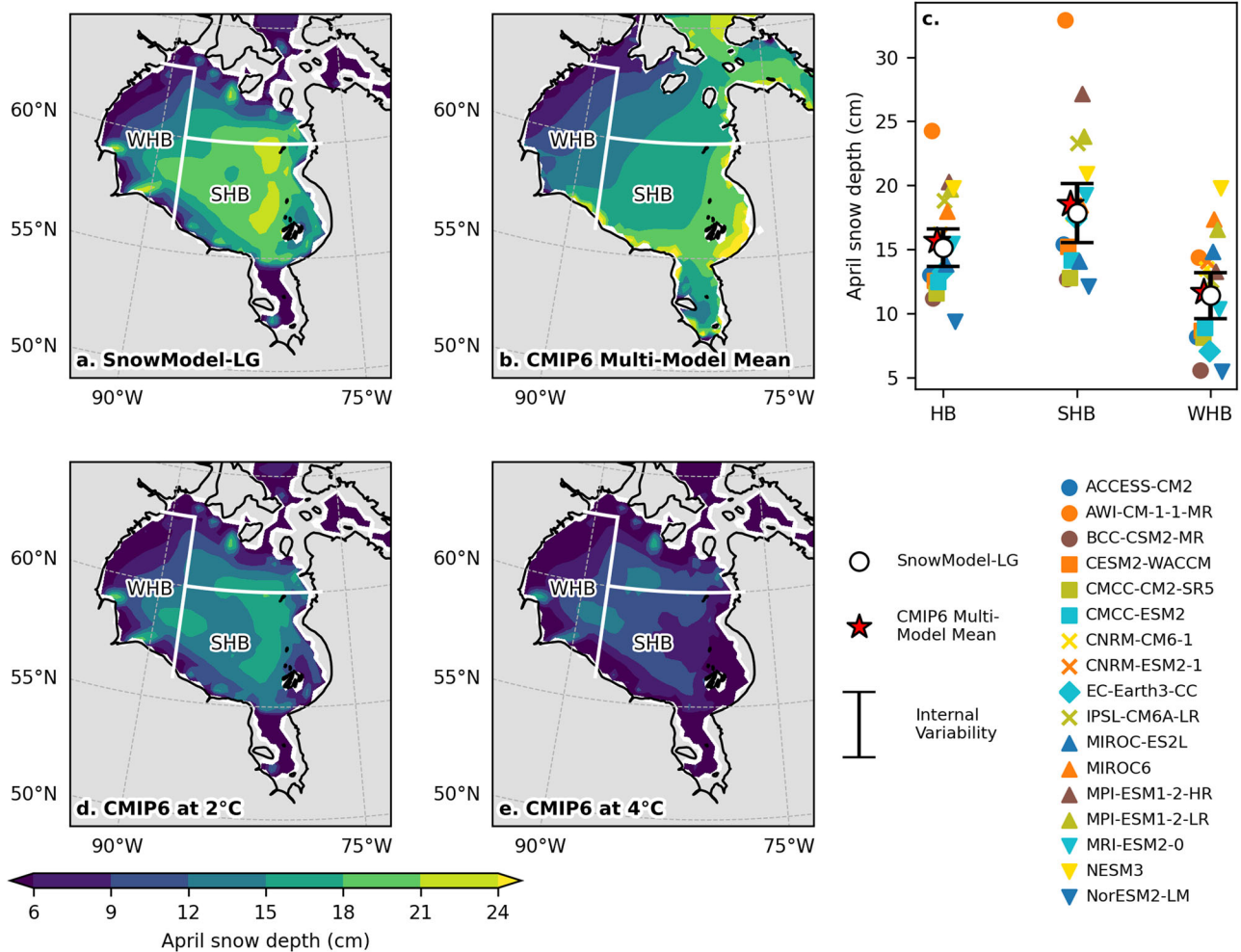
Fig. 6 | Multisource averages of April snow depth (1981-2021). April average snow depth in **a** the MERRA2-based snow depth (SnowModel-LG) and **b** the CMIP6 multi-model mean (no weighting or adjusting). **c** Regional averages of April snow depth for individual models (colored dots) compared to the SnowModel-LG (white), with internal variability estimated from the 30-member ensemble from MPI-ESM1-2-LR. Projections of future April snow depth using a bias-adjusted average are presented for **d** 2 °C and **e** 4 °C of global warming with respect to 1850–1900.

The above analysis however is based on a mean snow depth value at coarse spatial resolution and the relationship between average snow depth as indicated by satellite data products or climate models, and the presence of adequately deep snow at a finer scale, particularly on coastal landfast ice, is uncertain. This relationship will be influenced by local factors such as sea ice roughness (i.e. ridges) and prevailing wind patterns[34–36]. Thinner and more mobile ice may result in greater ice compaction, providing ridges around which snow can accumulate, providing enough snow for birth lairs, but this cannot be quantified in current satellite- and model-based snow depth estimates. Nevertheless, we can assume that if there is less snow accumulation over level ice there is less snow available to drift.

On the other hand, it is not only the reduced snow accumulation that is worrisome; more of the precipitation will also start to fall as rain under continued warming[37]. Examples of newborn ringed seal pups lying exposed on bare ice because their birth lairs had been washed away by unseasonably early rain (9–10 April) have been recorded[38]. Similar early rains will likely become more frequent with continued warming. Premature collapse of polar bear maternity dens on land because of unseasonably early rain is also a concern[1,39].

Discussion

Hudson Bay polar bears already experience some of the longest ice-free conditions of their species. Typically, the bears came ashore from late June to early August and remained until the ice reappeared in late November to early December[40]. However, during this last decade, the ice-free period has been 24 to 34 days longer than in 1981-1989 within SHB and 28 to 31 days longer in WHB, depending on which sea ice concentration algorithm is used to define the IFP (Fig. 1). Despite the longer IFP, earlier studies suggested that adult male numbers remained stable from 2009 to 2014, in part because they access a more variable diet, including the much larger (though less numerous) bearded seals[41]. In addition, their large size enables them to steal and benefit nutritionally from seal kills made by smaller bears[42]. Based on historical polar bear weights, rapid reductions in adult male survival would be expected once fasting expands to 200 days, although adult male weights, and therefore this threshold, have declined in recent decades[18]. Based on comparisons to location data collected via satellite telemetry from transmitting polar bear collars, a fasting period of 200 days equates to an IFP of 218 days (Supplementary Fig. 2).

Sub-adults[7,12,43] and adult females[44] are more sensitive to changes in sea ice phenology likely due to their smaller body size and greater reliance on the small ringed seal for prey, but possibly also because of having some of their kills stolen by larger bears. In WHB, decreased survival of juveniles, subadults and females was previously found to be significantly correlated with earlier ice retreat[12]. In the Canadian High Arctic, it was estimated that approximately 2/3 of the energy a polar bear needs for the year is taken in during the spring and early summer[45], primarily because that is when large numbers of ringed seal pups, which are 50% fat and less experienced at evading predators, become available[46]. Although similar assessments have not been made in WHB, it is likely that the overall pattern of strong

dependence of polar bears on young ringed seal pups in late spring and early summer would be similar, if only because there are no other sources of so much potential energy readily available at any other time of year. Thus, the continued shifting of the ice retreat from early (late) July towards mid-June (early July) under 2 °C of global warming will likely stimulate an increase in food-related stress, resulting in higher mortality of younger and female bears and a reduction of their reproductive potential. Importantly, every day of earlier sea ice breakup will have a much greater negative effect on polar bears than a delay in freeze-up because of the greater availability and vulnerability of ringed seal pups to predation in spring.

Compared to the population within WHB, the population of bears within SHB appeared relatively stable[47,48], despite evidence of declining body condition[44]. The reasoning for better demographic stability appears to be a result of the prevailing winds moving the ice southwards[49], such that the ice remains until late June/early July so that feeding opportunities have not been significantly reduced as early as they were further north in WHB. However, updated assessments have confirmed declines in body condition and a 17% decline in numbers of the SHB population between 2011 and 2016, probably as a result of less sea ice during the peak feeding period of late spring/early summer[50]. Thus the projected longer IFP in SHB may further reduce population numbers in the region in the future.

The planet has already exceeded 1 °C of global warming, with estimates for 2022 coming in at 1.26 °C[51] and the World Meteorological Organization (WMO) suggests a 66% chance that annual global temperatures will reach 1.5 °C above pre-industrial levels in the next 5 years[52]. While 1.5 °C is the aspirational target of the Paris Agreement, a legally binding international treaty on climate change adopted in 2015, 2.0 °C is considered the "hard limit"[53]. Studies suggest that at 165 days of fasting (which we estimate at 183 ice-free days; around 2 °C for SHB and 2.5 °C for WHB), 16% of healthy adult male polar bears would perish from starvation[7,54], with this rate increasing to 18 to 24% at 180 days of fasting (198 ice-free days; around 2.5 °C for SHB and 3 °C for WHB)[7]. Based on the average weight of adult male polar bears, Molnár et al. (2020)[18] estimated a historical (1989–1996) survival impact threshold of 200 fasting days (equivalent to 218 ice-free days). However, deteriorating body conditions had lowered that threshold to 171 fasting days (or 189 ice-free days) by 2007. In other words, our results suggest that adult male polar bear survival impact thresholds range from 183 to 218 ice-free days, but the lower end of estimates is likely most relevant today. Using that lower threshold, the global warming limit for supporting adult male polar bears is about 2.1 °C (1.6 °C) for SHB and about 2.6 °C (2.2 °C) for WHB (Fig. 4). Note that if bias-correction or weighting is not performed, the outlook would be more pessimistic: 1.5 °C for SHB and 2.0 °C for WHB (Supplementary Table 2. More concerning for overall population health is that after 117 days of fasting (135 ice-free days; experienced frequently since the late 1990s; Supplementary Fig. 2), recruitment of cubs is impacted due to the mother's reduced ability to provide milk[18]. Further, if spring break-up occurs one to two months earlier than the 1990s, it has been estimated that 40–73% and 55–100% of females could fail to reproduce, respectively, due to the extended fasting period and reduced feeding opportunities[55]. This suggests that SHB and WHB already cannot support long-term (sustainable) recruitment.

However, sea ice conditions are not the only important factor. The projected losses of snow cover will likely have similar implications, not only for polar bear denning but also for the creation and stability of ringed seal birth lair habitat and the availability of pups for polar bears to prey on. The survival of ringed seals has already been shown to be negatively affected by extreme sea ice loss[33]. In the southern Beaufort Sea, major but relatively short-term (1–2 year) declines in ringed seal productivity from natural causes immediately resulted in major but similarly short-term reductions in polar bear reproductive success[56]. However, because the significant reduction in ringed seal reproduction was relatively brief, population consequences for both ringed seals and polar bears was also brief. From these observations, it is clear that a significant long-term decline in ringed seal productivity in Hudson Bay, for whatever reason, would be devastating for the resident populations of polar bears.

Given the continued environmental changes to the Hudson Bay region documented already it is imperative to also understand what the future will hold for the livelihoods of those that live and work in the region. Inuit rely on traditional harvesting for social, economic, and cultural reasons and will be impacted by dramatic ecosystem shifts. As such they have vested interest in the health of the species that live there.

Part of the motivation for this study was that large biases in CMIP6 models toward over-estimating the IFP in Hudson Bay[3] could lead to an overly pessimistic prediction for declining polar bear habitat. If we persist with heavy use of fossil fuels and a high emission scenario (SSP3-7.0 or SSP5-8.5), global warming will likely exceed 4 °C before the end of this century. At 4 °C of warming, or even 3 °C, IFPs are prohibitively long to support adult polar bears even after applying a bias correction or model weighting scheme. Given recent declines in adult polar bear weight, habitat loss may become too great to sustain adult polar bears in SHB should global warming exceed the Paris Agreement's "hard limit" of 2 °C. Note that without accounting for model bias, extirpation would occur as soon as 1.5 °C of warming (Supplementary Table 2), so our results provide a relatively optimistic projection in this regard. However, we may already have surpassed a threshold of insufficient cub recruitment in both regions, which will have cascading impacts on population numbers.

While it is difficult to provide a hard-limit of IFP before extirpation of WHB or SHB polar bear populations occurs, confronted with these threats, proactive measures are imperative. Reducing the use of fossil fuels and advocating for sustainable development and climate adaptation initiatives could serve as initial steps in alleviating the pressure on marine mammals in the region.

Methods
Data Sets
In this study we rely on both sea ice and air temperatures from observations and the CMIP6 archive. Our reference time-series of sea ice phenology is based on the long-term passive microwave satellite data record from which sea ice concentration (SIC) is derived using two different algorithms Bootstrap[57] and NASA Team[58]. Both datasets are produced from October 1978 to present at 25-km horizontal resolution (Polar Stereographic North grid) with daily temporal resolution (2-day resolution prior to August 1987). Missing days prior to August 1987 are filled by averaging fields of the day immediately before and the day immediately after the data gap. Historical temperature data from 1850 to 2022 come from the instrument-based Berkeley Earth Surface Temperatures (BEST) Global Monthly Land + Ocean dataset[59], which has a horizontal resolution of 1 degree latitude and longitude.

Snow depth is harder to observe, though satellite estimates are available over first-year sea ice every 5 days in winter[60]. Another option is an atmospheric reanalysis-based data product SnowModel-LG[61], which provides daily snow depths for the Arctic, including Hudson Bay. We evaluated both the satellite- and reanalysis-based snow depth products, using SnowModel-LG forced with NASA's MERRA2 reanalysis[62], finding that while there is general agreement in mean snow depth during spring (Supplementary Fig. 1), they disagree strongly in trends. The microwave record has many missing values depending on year, in part because if there is a large change from day-to-day in the derived snow depth, the values are set to missing. Another limitation is that liquid water in the snowpack will lead to strong biases in retrieved snow depths and may be additionally influenced by surface roughness changes. SnowModel-LG has been evaluated against buoy data, magnaprobe data and Operational Ice Bridge (OIB) retrieved snow depths across the Arctic Ocean and was found to perform reasonably well[63] yet the accuracy of the product has not been evaluated in Hudson Bay due to a dearth of in situ observations. Nevertheless, we rely on SnowModel-LG to assess snow on sea ice changes.

To calibrate the IFP to the polar bear fasting period (i.e., the period of time polar bears spend onshore), we use the onshore/offshore dates for polar bears reported in Fig. 2 of Cherry et al. (2013)[64]. These data are derived from satellite-linked radio tags attached to collars worn by polar bears and is a

widely used technique to monitor the movements of polar bears, playing a key role in conservation efforts[65].

Projections of future sea ice conditions, snow depth over sea ice, and surface temperature are made using twenty earth system models participating in CMIP6. Two experiments are used: the historical (1850-2014) experiment and shared socioeconomic pathway (SSP) 5-8.5 (2015-2100) which reaches an additional radiative forcing of 8.5 W/m² by the year 2100, and represents the scenario provided by CMIP6 with the highest emissions. The twenty models used in this study are those for which daily SIC and thickness are available for at least one ensemble member (replicate) for the historical and SSP5-8.5 experiments (Supplementary Table 1)). The nominal spatial resolution of these models ranges from 50 km to 250 km, meaning there are as few as 88 and 158 grid cells in WHB and SHB, respectively (in model MPI-ESM1-2-LR) and as many as 3247 and 3325 grid cells in WHB and SHB, respectively (in model CNRM-CM6-1-HR). The SSP5-8.5 record was chosen because all future projections are considered relative to the global annual mean surface temperature anomaly (with respect to 1850-1900), and SSP5-8.5 offers the widest range of future temperatures. For the snow depth we used the monthly fields and focused on the month of April, which is the latest month in winter for which sea ice cover exists throughout the entire record.

Sea Ice Phenology

For observations, the annual ice-free period (IFP) for each grid cell is defined using a SIC threshold applied to the satellite data record[2]. First, a 5-day moving average is applied to remove short-term variability. Second, for each year the day of ice retreat is defined as the last day SIC falls below 10% in summer and the day of ice advance is defined as the first day SIC rises above 10% in autumn. The IFP is the time between retreat and advance, meaning that period for which SIC is continuously below 10%. While a more relevant metric would include the ice thickness needed to support a polar bear, the lack of a daily sea ice thickness product that spanned the winter and summer meant we had to rely on SIC for the observational period.

However, choosing the right SIC threshold can be difficult in part because satellite passive-microwave based assessments of SIC may be underestimated by up to 50% especially when the snow is wet during the breakup period and when the water areas are covered by frazil and young ice during freeze-up[66]. Studies have suggested bears prefer greater than 50% ice cover[67,68], and come to shore when the SIC drops below 50%[69]. This is in part because fragmented ice and swimming results in more energy expenditure by the bears[56]. However, observational evidence has also shown that bears may linger on broken ice floes for a longer period before coming onshore. The best fit regression model for predicting when a bear comes on shore and leaves was 30% and 10% SIC (regional averaged), respectively[64]. Alternatively, the period for which sea ice extent is below 30% of its annual maximum has also been used[18]. Because the different grids in CMIP6 can lead to biases in sea ice extent measurements[27], we prefer defining retreat, advance, and IFP at a cell-by-cell scale first and then calculating a spatial average. More specifically, we find a close match between the 10% SIC threshold and the 30% sea ice extent threshold use by Molnár et al.[18] (Supplementary Fig. 2). We acknowledge that this can include either a solid or quite fragmented ice cover depending on the snow and thin ice conditions.

Despite slight differences in overall mean IFPs, the spatial patterns are mostly consistent between algorithms with the exception of coastal areas where the NASA Team algorithm shows a larger increase in the IFP between the two decades (Fig. 1) The NASA Team algorithm can be biased towards lower SIC than Bootstrap when the ice is not snow covered or in the presence of thin ice, as the tie-points for the 100% SIC are based on snow-covered multiyear ice. Compared to 1981-1989, the ice-free period during the last decade (2012–2021) is 24 to 34 days longer in SHB and 28 to 31 days longer in WHB, depending on which SIC algorithm is used. Averaging together the IFP from the two algorithms, the WHB IFP averages 18 days longer than the onshore period for polar bears, as measured using satellite telemetry data[64]. Satellite telemetry involves the use of satellite-linked radio tags attached to

collars and is a widely used technique to monitor the movements of polar bears, playing a key role in conservation efforts[65]. Years used for this comparison are 1991–1992, 1994–1997, 2005–2009.

We additionally compute the climatological average, trend ($\Delta IFP / \Delta t$), and temperature sensitivity of IFP ($\Delta IFP / \Delta T$) from 1979 to 2021 using ordinary least-squares regression. Temperature (T) is the global annual mean surface temperature from BEST. These quantities are shown in Fig. 2.

For CMIP6 models, we tested computing the IFP using two thresholds: 10% SIC or 10 cm sea ice thickness. The former is identical to the observational method; however, the latter metric more closely matches the average observed ice-free period during 1979–2021 (Fig. 2). Therefore, IFP based on sea ice thickness is the primary metric used for future projections. The threshold of 10 cm is the minimum possible sea ice thickness for some frazil ice schemes[25]. Internal variability of averages, trends, and temperature sensitivity is measured as two times the standard deviation of the MPI-ESM1-2-LR ensemble, which has 30 members for each experiment. Finally, note that in a few models at high warming levels (4 °C and higher), some grid cells in Hudson Bay are ice-free for entire years. The IFP is 365 (or 366) days in such cases, but the retreat and advance days are invalid. Retreat and advance are ignored during spatial averaging in such cases. Therefore, although IFP = advance day - retreat day, the spatially averaged IFP may be slightly longer than the difference of spatially averaged advance day and spatially averaged retreat day in a few models at high warming levels.

Correcting future projections

Two methods are used to construct a projection of future ice-free periods in western Hudson Bay (WHB), which encompasses the area west of 88°W and south of 63°N, and southern Hudson Bay (SHB) which includes eastern Hudson Bay and James Bay (Fig. 2) (1) a single-member average of all 20 models after applying a bias adjustment (2) a performance-based weighted average of 49 simulations from the 20 models. For the single-member average, the first ensemble member ("replicate 1") is chosen whenever possible. For CESM2, replicate 1 only exists for the historical experiment, so replicate 4 is used instead. The bias adjustment is designed to eliminate bias in the average historical IFP. Using the BEST temperature data, the range of global annual surface temperature anomalies from the observational period (1979–2021) relative to 1850–1900 is 0.42 °C to 1.33 °C. Therefore, the bias ($B_{m,x}$) in IFP for a given model simulation (m) and location (x) is measured by averaging IFP for all years in the model simulation for which 0.42 °C < T_m < 1.33 °C (i.e., $IFP_{m,x}(T_m)$) and comparing to the observed IFP from 1979–2021 ($IFP_{o,x}$); Eq. (1).

$$B_{m,x} = IFP_{m,x}(T_m) - IFP_{o,x} \qquad (1)$$

$$IFPadj_{m,x,t} = IFP_{m,x,t} - B_{m,x} \qquad (2)$$

Note that "observed" means the average between Bootstrap and NASA Team. The bias is then subtracted from all future projections to acquire a bias-adjusted ice-free period ($IFPadj_{m,x,t}$). This method preserves any trend in the model, but any reported change is relative to the observed IFP 1979–2021. Adjusting based on the global temperature anomaly instead of time controls for bias in the rate of global warming (i.e., climate sensitivity) exhibited by several models[26].

Finally, the weighted average is constructed following the general method of Knutti et al.[70], which assigns less weight to a simulation if it compares poorly to observations or if it effectively duplicates another simulation in the ensemble. This second property recognizes that model simulations are not independent: many models share components, and several model experiments include multiple simulations. However, in our particular sample, two related models (MPI-ESM1-2-LR and MPI-ESM1-2-HR) were responsible for 50% of all simulations. Therefore, we first limited our weighting scheme to no more than seven ensemble members per model (taking the first seven). Doing this, no one model is responsible for more than 15% of the 49 simulations used in the weighting scheme.

The weighting scheme relies on a distance metric both between each pair of model simulations (S_{ij}) and between each model simulation and observations (D_i). For our study, "distance" is defined as the root-mean-square difference of 16 variables. Each variable is normalized by the median distance exhibited by all simulations, so each variable has about the same weight. The variables used include the average and trend of regional temperature and global temperature sensitivity of the ice-free period, advance day, and retreat day. Those eight variables are considered for both southern and western Hudson Bay regions. This combination of variables will give less weight to a model that does not match observed averages and changes to IFP in Hudson Bay. By including the temperature and temperature sensitivity, it will also give less weight if that model is getting the IFP correct for the wrong reason. However, by including IFP as well as retreat and advance day, sea ice has a larger impact on the final weights than temperature.

Weighting based on these distances has a Gaussian shape, with weight decreasing exponentially with distance (Eq. (3)). Two constants are needed to tune the sensitivity of the weighting scheme to the two possible goals: weighting by match to observations versus weighting by independence. A higher value of σ_D distributes weight more equally amongst models, whereas a smaller σ_D emphasizes the higher performing models. The importance of model independence increases with higher σ_S.

$$W_i = \exp\left(-\frac{D_i^2}{\sigma_D^2}\right) \times \left(1 + \sum_{j \neq i}^M \exp\left(-\frac{S_{i,j}^2}{\sigma_S^2}\right)\right) \qquad (3)$$

The weighting results presented here use $\sigma_D = 0.49$ and $\sigma_S = 0.50$. As in Knutti et al.[70], our results are only sensitive to the choice of σ_D. One way to assess the robustness of results is to perform a series of perfect-model experiments where, instead of training based on observations, the training is done using one of the model simulations as the reference. After training for the period 1979-2021, the other simulations are used to predict the IFP in the reference simulation for the period 2070-2099. This process is repeated for each simulation, and for a range of values of σ_D and σ_S. The results of this perfect model experiment show that for both western and southern Hudson Bay, lower values of σ_D lead to a higher correlation between predicted IFP and the true IFP (from reference model) for 2070-2099 (Supplementary Fig. 3). However, choosing a value of σ_D that is too low risks underestimating future projection uncertainty. When σ_D is below 0.4, fewer than 90% of perfect model experiments result in the true IFP value for 2070-2099 falling within the 5–95% confidence range derived from the weighting scheme, which indicates that any value below 0.4 is over-confident.

We selected 0.49 instead of 0.40 because of one additional concern: the risk of over-fitting to a single model. The five simulations from the MRI-ESM-2-0 model receive about 80% of the weight if $\sigma_D = 0.40$, because this model is by far the closest match to observations. Using 0.49 is the lowest we can go and have MRI-ESM-2-0 responsible for less than two-thirds of the weight. The end result is five MRI-ESM-2-0 simulations each having at least 8% of the weight (60% in total) and 10 other simulations each having at least 1% of the weight (Extended Data Fig. 4).

The sum of weights is always one, so the final equations for the weighted mean ($\overline{IFP}$; Eq. (4)) and standard error (IFP_{se}; Eq. (5)), where i represents each simulation in the set of $n = 49$ weighted simulations, are:

$$\overline{IFP} = \sum W_i IFP_i \qquad (4)$$

and

$$IFP_{se} = \left(\frac{\sum W_i \left(IFP_i - \overline{IFP}\right)^2}{(n-1)}\right)^{0.5} \qquad (5)$$

For projections of snow depth, we use only a bias-adjusted average, not a weighted average. The weighted average scheme we use requires a reference dataset for both the average and trend of the desired properties, and the satellite- and reanalysis-based snow depth data sets have poor agreement in their long-term trends. Therefore, snow depth was excluded from the weighting scheme, and no weighted average was calculated for snow depth.

Reporting summary
Further information on research design is available in the Nature Portfolio Reporting Summary linked to this article.

Data availability
The estimates of IFP, retreat, and advance from satellite are available from https://canwin-datahub.ad.umanitoba.ca/data/dataset/arctic-sea-ice-phenology-from-passive-microwave-satellite-retrievals, and the CMIP6 projections of IFP, retreat and advance are available from https://canwin-datahub.ad.umanitoba.ca/data/dataset/cmip6-hudson-bay-sea-ice-thickness-phenology. Original CMIP6 files (sea ice concentration, thickness, and snow depth) are available from any of the Earth System Grid Federation nodes (https://esgf.github.io/nodes.html). Polar bear onshore/offshore dates are from Cherry et al. (2013)[64]. SnowModel-LG snow depths are available from https://nsidc.org/data/nsidc-0758/versions/1.

Code availability
The related code for calculating retreat and advance and reproducing all figures is available from https://doi.org/10.5281/zenodo.4416124.

References
1. Stirling, I. & Derocher, A. Effects of climate warming on polar bears: a review of the evidence. *Glob. Chang. Biol.* **18**, 2694–2706 (2012).
2. Crawford, A., Stroeve, J., Smith, A. & Jahn, A. Arctic open-water periods are projected to lengthen dramatically by 2100. *Commun. Earth Environ.* **2**, 109 (2021).
3. Crawford, A. D., Rosenblum, E., Lukovich, J. V. & Stroeve, J. C. Sources of seasonal sea-ice bias for CMIP6 models in the Hudson Bay Complex. *Ann. Glaciol.* 1–18 https://doi.org/10.1017/aog.2023.42 (2023).
4. Andrews, J., Babb, D. & Barber, D. G. Climate change and sea ice: Shipping in Hudson Bay, Hudson Strait, and Foxe Basin (1980–2016). *Elementa* **6**, 1–23 (2018).
5. Laidre, K. L., Stirling, I., Estes, J. A., Kochnev, A. & Roberts, J. Historical and potential future importance of large whales as food for polar bears. *Front. Ecol. Environ.* **16**, 515–524 (2018).
6. Stempniewicz, L., Kulaszewicz, I. & Aars, J. Yes, they can: polar bears Ursus maritimus successfully hunt Svalbard reindeer Rangifer tarandus platyrhynchus. *Polar Biol.* **44**, 2199–2206 (2021).
7. Pilfold, N. W. et al. Mass loss rates of fasting polar bears. *Physiol. Biochem. Zool.* **89**, 377–388 (2016).
8. Gagnon, A. S. & Gough, W. A. Trends in the dates of ice freeze-up and breakup over Hudson Bay, Canada. *Arctic* **58**, 370–382 (2005).
9. Hochheim, K. P. & Barber, D. G. An update on the ice climatology of the Hudson Bay system. *Arct. Antarct. Alp. Res.* **46**, 66 – 83 (2014).
10. Derocher, A. E. & Stirling, I. Estimation of polar bear population size and survival in Western Hudson Bay. *J. Wildl. Manag.* **59**, 215–221 (1995).
11. Lunn, N. J., Stirling, I., Andriashek, D. & Kolenosky, G. B. Re-estimating the size of the polar bear population in Western Hudson Bay. *Arctic* **50**, 234–240 (1997).
12. Regher, E. V., Lunn, N. J., Amstrup, S. C. & Stirling, I. Effects of earlier sea ice breakup on survival and population size of polar bears in Western Hudson Bay. *J. Wildl. Manag.* **71**, 2673–2683 (2007).
13. Atkinson, S. N. et al. Aerial survey of the western hudson bay polar bear subpopulation 2021. final report. Tech. Rep., Government of Nunavut, Department of Environment, Wildlife Research Section (2022).

14. Lunn, N. J. et al. Demography of an apex predator at the edge of its range: impacts of changing sea ice on polar bears in Hudson Bay. *Ecol. Appl.* **26**, 1302–1320 (2016).

15. Atkinson, S. N. et al. A novel mark-recapture-recovery survey using genetic sampling for polar bears Ursus maritimus in Baffin Bay. *Endanger. Species Res.* **46**, 105–120 (2021).

16. IPCC. Summary for Policymakers. In Masson-Delmotte, V.*et al*. (eds.) *Climate Change 2021: The Physical Science Basis. Contribution of Working Group I to the Sixth Assessment Report of the Intergovernmental Panel on Climate Change* (Cambridge University Press, 2021).

17. Eyring, V. et al. Overview of the Coupled Model Intercomparison Project Phase 6 (CMIP6) experimental design and organization. *Geosci. Model Dev.* **9**, 1937–1958 (2016).

18. Molnár, P. K. et al. Fasting season length sets temporal limits for global polar bear persistence. *Nat. Clim. Chang.* **10**, 732–738 (2020).

19. Stirling, I. & Parkinson, C. Possible effects of climate warming on selected populations of polar bears (Ursus maritimus) in the Canadian Arctic. *Arctic*. **59**, 261–275 (2006).

20. Pilfold, N., Derocher, A., Stirling, I. & Richardson, E. Polar bear predatory behaviour reveals seascape distribution of ringed seal lairs. *Popul. Ecol.* **56**, 129–138 (2014).

21. Fergurson, S. H., Taylor, M. K. & Messier, F. Influence of sea ice dynamics on habitat selection by polar bears. *Ecology* **81**, 761–772 (2000).

22. Smith, T. G. Polar bear predation of ringed and bearded seals in the land-fast sea ice habitat. *Can. J. Zool.* **58**, 2201–2209 (1980).

23. Gjertz, I. & Lydersen, C. Polar bear predation on ringed seals in the fast-ice of Hornsund, Svalbard. *Polar Res.* **4**, 65–68 (1986).

24. Rode, K. et al. Seal body condition and atmospheric circulation patterns influence polar bear body condition, recruitment, and feeding ecology in the Chukchi Sea. *Glob. Chang. Biol.* **27**, 2684–2701 (2021).

25. Keen, A. et al. An inter-comparison of the mass budget of the Arctic sea ice in CMIP6 models. *Cryosphere* **15**, 951–982 (2021).

26. Tokarska, K. B. et al. Past warming trend constrains future warming in CMIP6 models. *Sci. Adv.* **6**, eaaz9549 (2020).

27. Notz, D. & Community, S. Arctic Sea Ice in CMIP6. *Geophys. Res. Lett.* **47** (2020).

28. Sciullo, L., Thiemann, G. W., Lunn, N. J. & Ferguson, S. H. Intraspecific and temporal variability in the diet composition of female polar bears in a seasonal sea ice regime. *Arct. Sci.* **3**, 672–688 (2017).

29. Bajzak, C., Bernhardt, W., Mosnier, A. & Hammill, M. Habitat use by harbour seals (Phoca vitulina) in a seasonally ice-covered region, the western Hudson Bay. *Polar Biol.* **36**, 477–491 (2013).

30. Smith, T. G. & Stirling, I. The breeding habitat of the ringed seal (Phoca hispida). The birth lair and associated structures. *Can. J. Zool.* **9**, 1297–1305 (1975).

31. Furgal, C., Innes, S. & Kovacs, K. Characteristics of ringed seal, Phoca hispida, subnivean structures and breeding habitat and their effects on predation. *Can. J. Zool.* **74**, 858–874 (1996).

32. Lydersen, C. Status and biology of ringed seals (Phoca hispida) in Svalbard. *NAMMCO Sci. Publ.* **1**, 46–62 (1998).

33. Ferguson, S. H. et al. Demographic, ecological, and physiological responses of ringed seals to an abrupt decline in sea ice availability. *PeerJ* **5**, e2957 (2017).

34. Iacozza, J. & Ferguson, S. H. Spatio-temporal variability of snow over sea ice in western Hudson Bay, with reference to ringed seal pup survival. *Polar Biol.* **37**, 817–832 (2014).

35. Iacozza, J. & Barber, D. G. An examination of the distribution of snow on sea-ice. *Atmos. Ocean* **37**, 21–51 (1999).

36. Sturm, M., Holmgren, J. & Perovich, D. K. Winter snow cover on the sea ice of the Arctic Ocean at the Surface Heat Budget of the Arctic Ocean (SHEBA): Temporal evolution and spatial variability. *J. Geophys. Res. Ocean.* **107**, SHE 23–1–SHE 23–17 (2002).

37. McCrystall, M. R., Stroeve, J., Serreze, M., Forbes, B. C. & Screen, J. A. New climate models reveal faster and larger increases in Arctic precipitation than previously projected. *Nat. Commun.* **12**, 6765 (2021).

38. Stirling, I. & Smith, T. G. Implications of warm temperatures and an unusual rain event for the survival of ringed seals on the coast of Southeastern Baffin Island. *Arctic* **57**, 59–67 (2004).

39. Clarkson, P. L. & Irish, D. Den collapse kills female polar bear and two newborn cubs. *Arctic*. **44**, 83–84 (1991).

40. Ramsay, M. A. & Stirling, I. Reproductive biology and ecology of female polar bears (ursus maritimus). *J. Zool.* **214**, 601–633 (1988).

41. Thiemann, G. W., Iverson, S. J. & Stirling, I. Polar bear diets and arctic marine food webs: insights from fatty acid analysis. *Ecol. Monogr.* **78**, 591–613 (2008).

42. Stirling, I. Midsummer observations on the behavior of wild polar bears (Ursus maritimus). *Can. J. Zool.* **52**, 1191–1198 (1974).

43. Rode, K. D., Amstrup, S. C. & Regehr, E. V. Reduced body size and cub recruitment in polar bears associated with sea ice decline. *Ecol. Appl.* **20**, 768–782 (2015).

44. Obbard, M. et al. Trends in body condition in polar bears (Ursus maritimus) from the Southern Hudson Bay subpopulation in relation to changes in sea ice. *Arct. Sci.* **2**, 15–32 (2016).

45. Stirling, I. & Øritsland, N. A. Relationships between estimates of ringed seal and polar bear populations in the Canadian Arctic. *Can. J. Fish. Aquat. Sci.* **52**, 2594–2612 (1995).

46. Stirling, I. & McEwan, E. H. The caloric value of whole ringed seals (Phoca hispida) in relation to polar bear (Ursus maritimus) ecology and hunting behavior. *Can. J. Zool.* **53**, 1021–1026 (1975).

47. Obbard, M. E. et al. Temporal trends in the body condition of Southern Hudson Bay polar bears. *Clim. Chang. Res. Inf. Note* **3**, 1–8 (2006).

48. Obbard, M. E. Southern Hudson Bay polar bear project 2003–2005, Final report. Tech. Rep., Ontario Ministry of Natural Resources, Peterborough, Ontario, Canada (Obbard2008).

49. Kirillov, S. et al. Atmospheric forcing drives the winter sea ice thickness asymmetry of Hudson bay. *J. Geophys. Res. Ocean.* **125**, e2019JC015756 (2020).

50. Obbard, M. E. et al. Re-assessing abundance of Southern Hudson Bay polar bears by aerial survey: Effects of climate change at the southern edge of the range. *Arct. Sci.* **4**, 634–655 (2018).

51. Bettz, R. et al. Approaching 1.5 °C: how will we know we've reached this crucial warming mark? *Nature* **624**, 33–35 (2023).

52. WMO. WMO Global Annual to Decadal Climate Update (Target years: 2023-2027). Tech. Rep., World Meteorological Organization (WMO) (2023).

53. Meinshausen, M., Lewis, J. & McGlade, C. et al. Realization of Paris Agreement pledges may limit warming just below 2C. *Nature* **604**, 304–309 (2022).

54. Robbins, C. T., Lopez-Alfaro, C., Rode, K. D., Tien, i & Nelson, O. L. Hibernation and seasonal fasting in bears: the energetic costs and consequences for polar bears. *J. Mammal.* **93**, 1493–1503 (2012).

55. Molnár, P. K., Derocher, A. E., Klanjscek, T. & Lewis, M. A. Predicting climate change impacts on polar bear litter size. *Nat. Commun.* **2**, 186 (2011).

56. Stirling, I. Polar bears and Seals in the Eastern Beaufort Sea and Amundsen Gulf: a synthesis of population trends and ecological relationships over three decades. *Arctic* **55**, 59–76 (2002).

57. Comiso, J. C. Bootstrap Sea Ice Concentrations from Nimbus-7 SMMR and DMSP SSM/I-SSMIS, Version 3 (2017).

58. Cavalieri, D. J., Parkinson, C. L., Gloersen, P. & Zwally, H. Sea Ice Concentrations from Nimbus-7 SMMR and DMSP SSM/I-SSMIS Passive Microwave Data, Version 1 (1996).

59. Rohde, R., Muller, R., Jacobsen, R., Perlmutter, S. & Mosher, S. Berkeley earth temperature averaging process. *Geoinform. Geostat.: Overview* **1** (2013).

60. Markus, T. & Cavalieri, D. J. Snow Depth Distribution Over Sea Ice in the Southern Ocean from Satellite Passive Microwave Data. In

Jeffries, M. O. (ed.) *Antarctic Sea Ice: Physical Processes, Interactions and Variability*, Antarctic Research Series, 19–39 (Wiley Online Library, 1998).

61. Liston, G. E. et al. A Lagrangian snow-evolution system for sea-ice applications (SnowModel-LG): Part I—Model Description. *J. Geophys. Res. Ocean.* **125**, e2019JC015913 (2020).

62. Gelaro, R. et al. The modern-era retrospective analysis for research and applications, Version 2 (MERRA-2). *J. Clim.* **30**, 5419 – 5454 (2017).

63. Stroeve, J. et al. A Lagrangian snow evolution system for sea ice applications (SnowModel-LG): Part II—Analyses. *J. Geophys. Res. Ocean.* **125**, e2019JC015900 (2020).

64. Cherry, S. G., Derocher, A. E., Thiemann, G. W. & Lunn, N. J. Migration phenology and seasonal fidelity of an Arctic marine predator in relation to sea ice dynamics. *J. Anim. Ecol.* **82**, 912–921 (2013).

65. Laidre, K. et al. The Role of Satellite Telemetry Data in 21st Century Conservation of Polar Bears (Ursus maritimus). *Front. Mar. Sci.* 9 (2022).

66. Agnew, T. & Howell, S. The use of operational ice charts for evaluating passive microwave ice concentration data. *Atmos.-Ocean* **41**, 317–331 (2003).

67. Durner, G. M. et al. Predicting 21st-century polar bear habitat distribution from global climate models. *Ecol. Monogr.* **79**, 25–58 (2009).

68. Stirling, I., Lunn, N. J. & Iacozza, J. Long-term trends in the population ecology of Polar Bears in Western Hudson bay in relation to climatic change. *Arctic* **52**, 294–306 (1999).

69. Derocher, A. E., Lunn, N. J. & Stirling, I. Polar bears in a warming climate. *Integr. Comp. Biol.* **44**, 163–176 (2004).

70. Knutti, R. et al. A climate model projection weighting scheme accounting for performance and interdependence. *Geophys. Res. Lett.* **44**, 1909–1918 (2017).

Acknowledgements

Author contributions

J. Stroeve conceived the idea for the paper, wrote the manuscript, and evaluated the passive microwave and SnowModel-LG snow depths. A. Crawford processed the sea ice phenology data from the satellite and the CMIP6 models and edited the manuscript. I. Stirling, G. York, and S. Ferguson provided input on the impacts of future sea ice and snow cover changes on polar bears and seals. L. Archer, D. Babb, and R. Mallet provided additional editing for clarity and accuracy.

Competing interests

The authors declare no competing interests.

Additional information

Supplementary information The online version contains supplementary material available at https://doi.org/10.1038/s43247-024-01430-7.

Correspondence and requests for materials should be addressed to Julienne Stroeve.

Peer review information *Communications Earth and Environment* thanks the anonymous reviewers for their contribution to the peer review of this work. Primary Handling Editors: Clare Davis. A peer review file is available.

Reprints and permissions information is available at http://www.nature.com/reprints

Publisher's note Springer Nature remains neutral with regard to jurisdictional claims in published maps and institutional affiliations.